Supporting information

A green strategy for selective recovery of valuable metals from spent lithium-ion batteries through waste graphite-assisted sulfation process

Minyu He [a, b], Fagen Zhou [a], Sohrab Rohani [c], Charles Q. Jia [b], Dong Wang [a,*], Wenhao Yu [a], Liumei Teng [a], Fei Meng [d], Qingcai Liu [a], Weizao Liu [a,*]

[a] College of Materials Science and Engineering, Chongqing University, Chongqing 400044, China

[b] Department of Chemical Engineering and Applied Chemistry, University of Toronto, Toronto M5S 3E5, Canada

[c] Department of Chemical and Biochemical Engineering, Western University, London, Ontario, Canada

[d] School of Metallurgy and Power Engineering, Chongqing University of Science and Technology, Chongqing 401331, China

*Corresponding author: wangdong2023@cqu.edu.cn (D. Wang); liuwz@cqu.edu.cn (W. Liu).

Supporting Information Content

19 pages (including the cover page)

17 Figures

6 Tables

3 Text

Figure S1. X-ray diffraction patterns of the cathode powder.

technologies (NR is not required).

Table S4. Value of recycled materials ($/kg).

Table S5. Material recovered from recycling process (kg/kg spent battery).

Table S6. The potential revenue of three recycling processes.

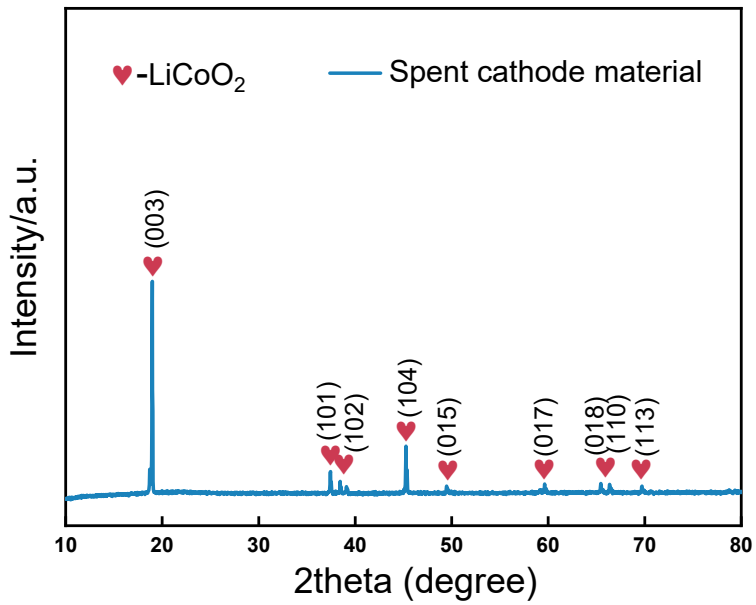

Figure S1. X-ray diffraction patterns of the cathode powder.

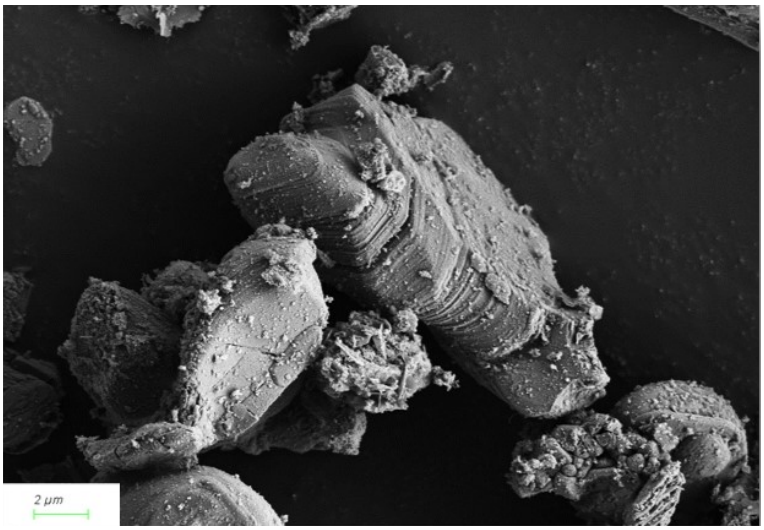

Figure S2. SEM analysis of the cathode powder.

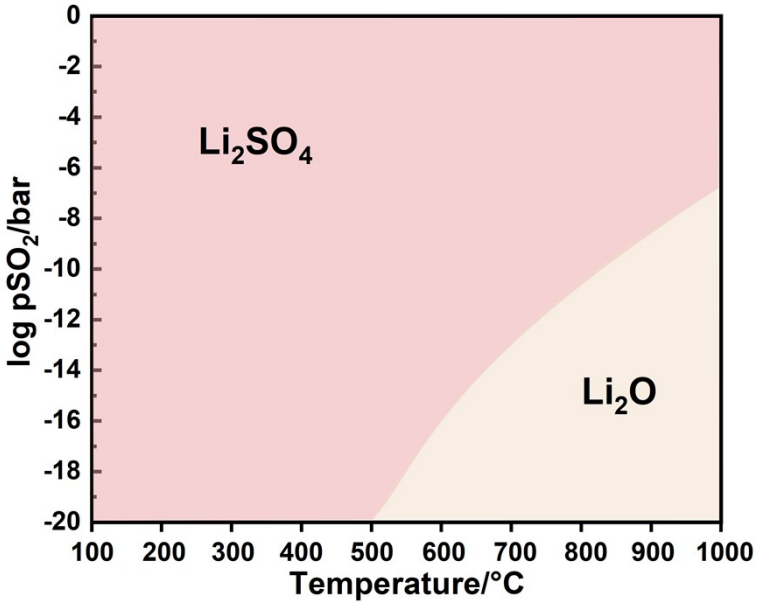

Figure S3. Stability diagram for Li-S-O (constant value: pO_2 (bar) = 0.21, air atmosphere), all thermodynamic calculation diagrams were obtained using HSC9.0 software.

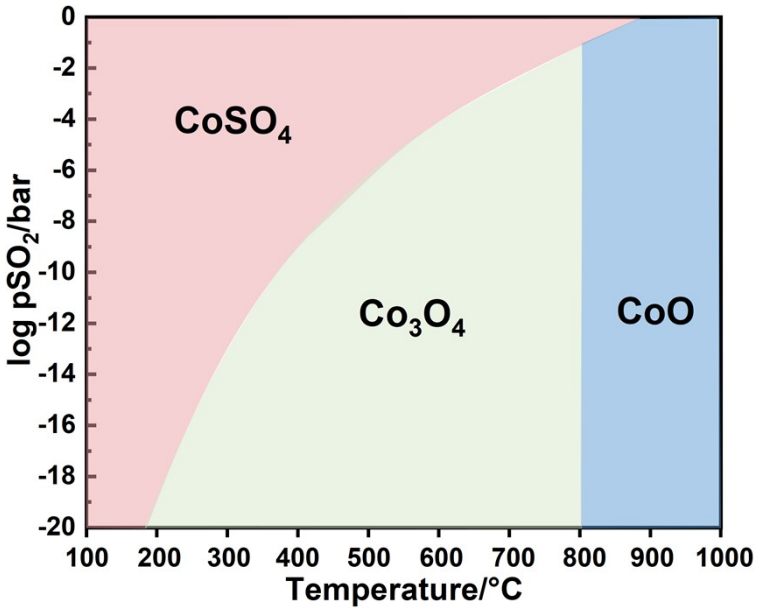

Figure S4. Stability diagram for Co-S-O (constant value: pO_2 (bar) = 0.21, air atmosphere), all thermodynamic calculation diagrams were obtained using HSC9.0 software.

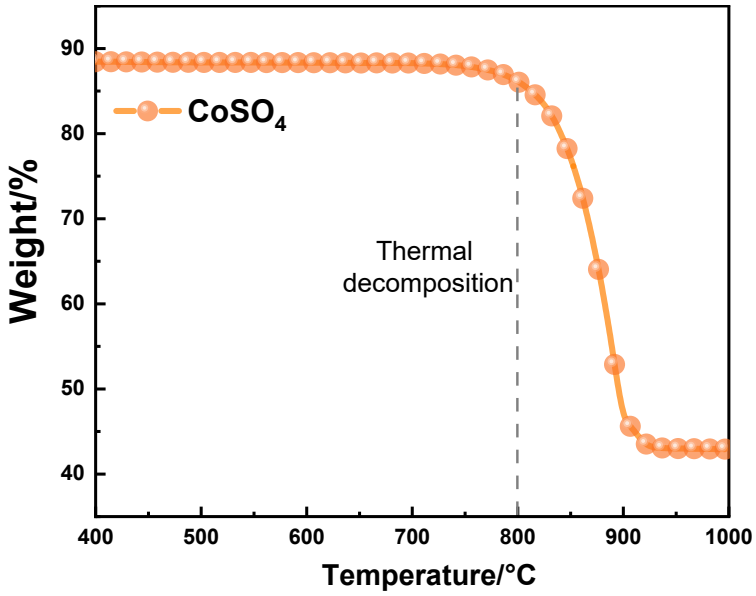

Figure S5. TG curve of decomposed of pure cobalt sulfate.

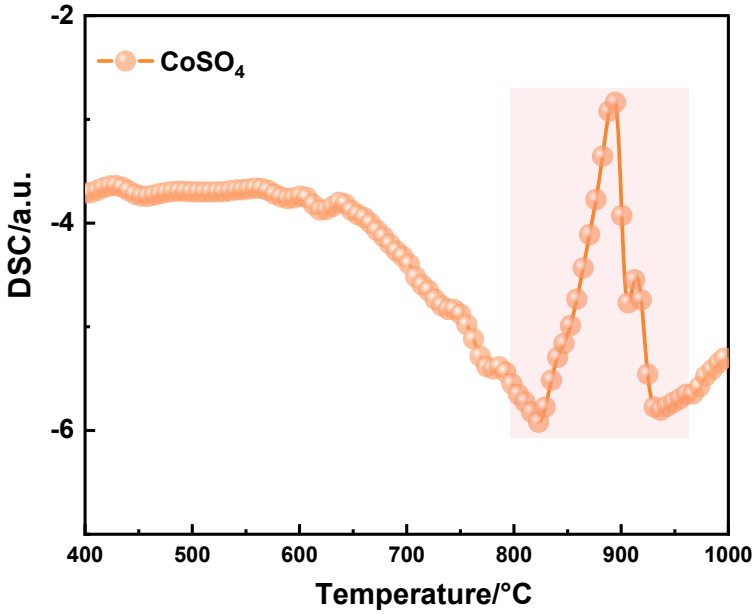

Figure S6. DSC curve of Decomposed of pure cobalt sulfate.

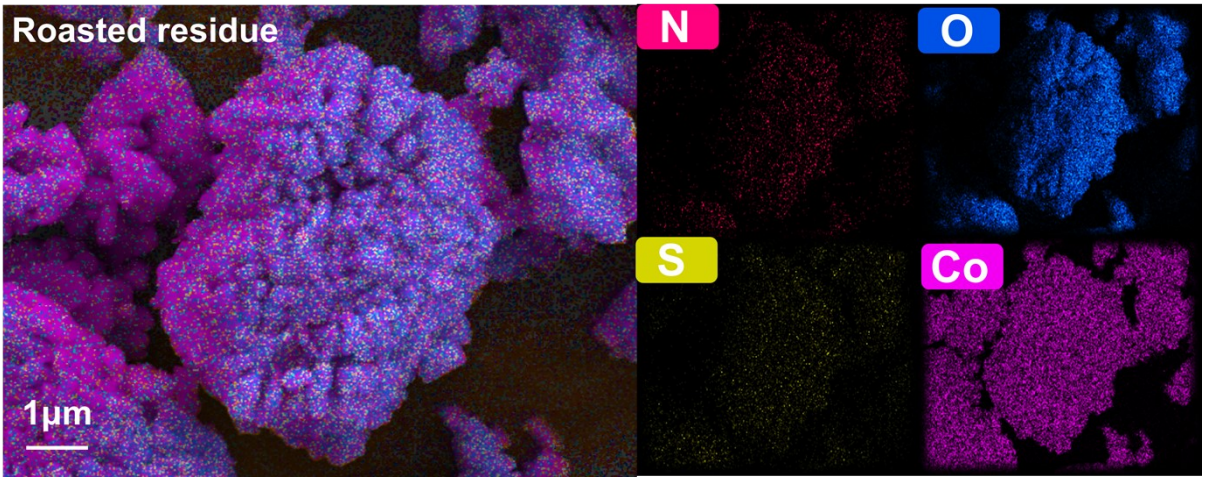

Figure S7. SEM-EDS analysis of obtained roasted residue.

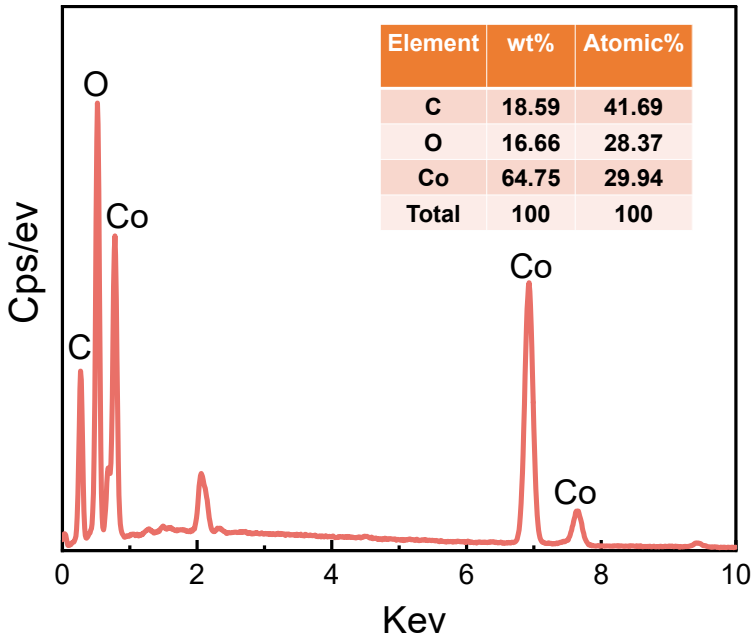

Figure S8. EDS analysis and atomic proportions of the resulting roasted residue.

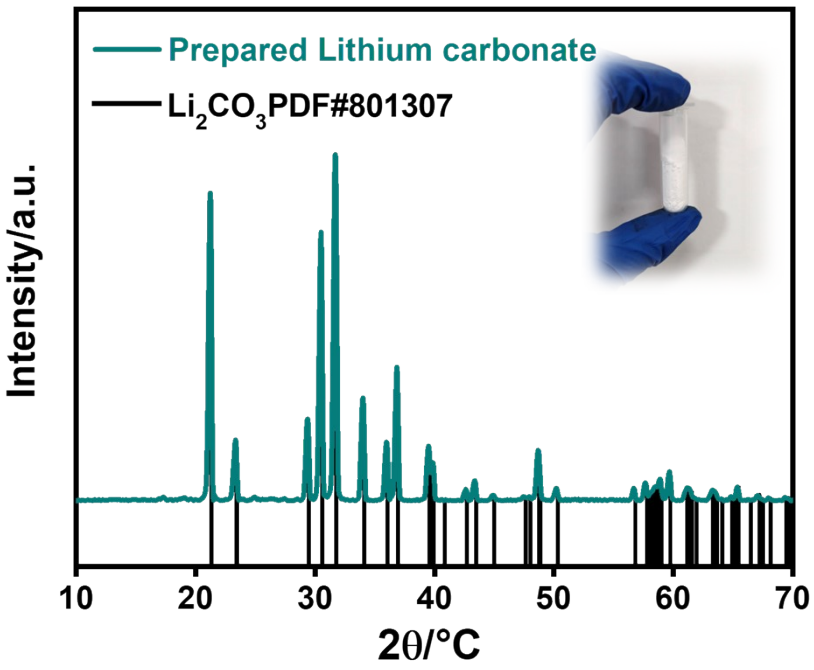

Figure S9. XRD analysis of the obtaining lithium carbonate.

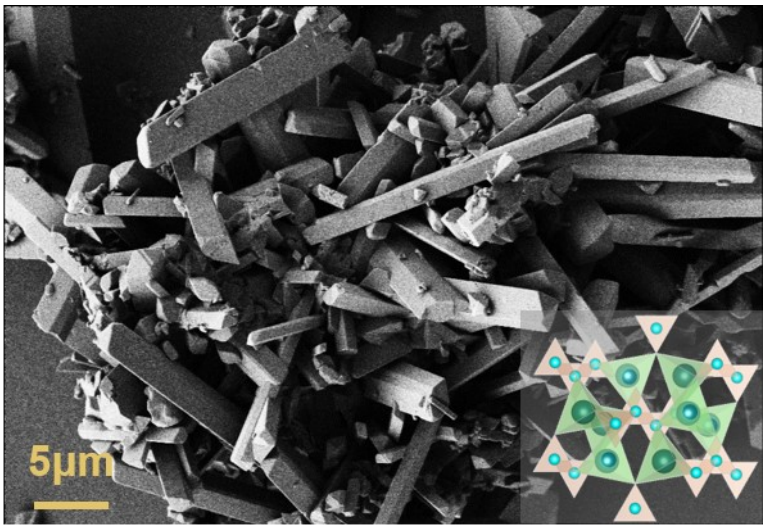

Figure S10. SEM analysis of the obtaining lithium carbonate.

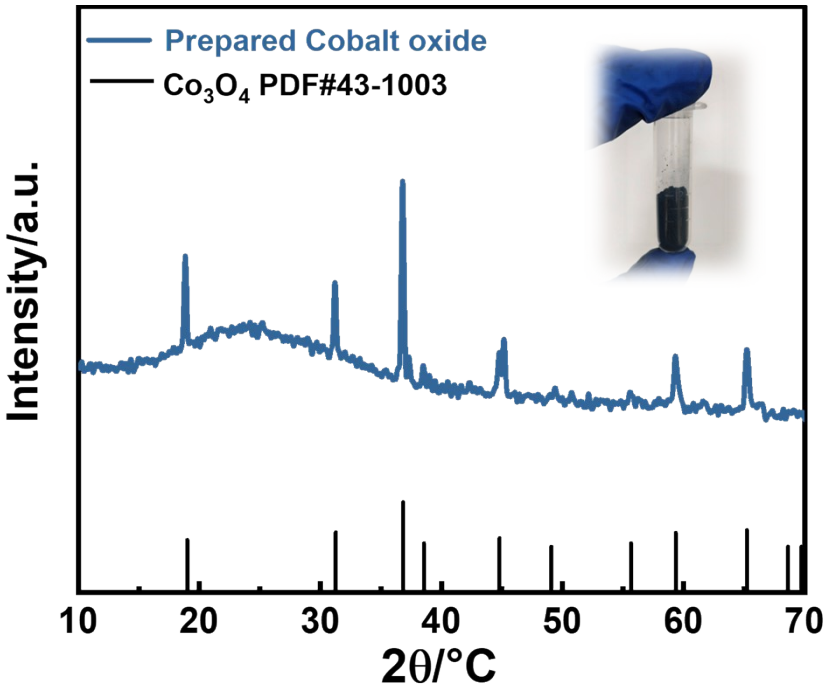

Figure S11. XRD analysis of the obtaining the Co_3O_4 particles.

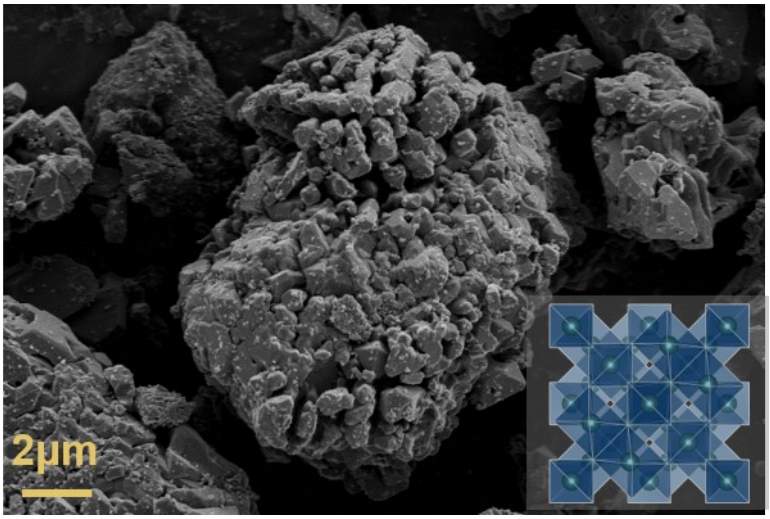

Figure S12. SEM analysis of the obtaining the Co_3O_4 particles.

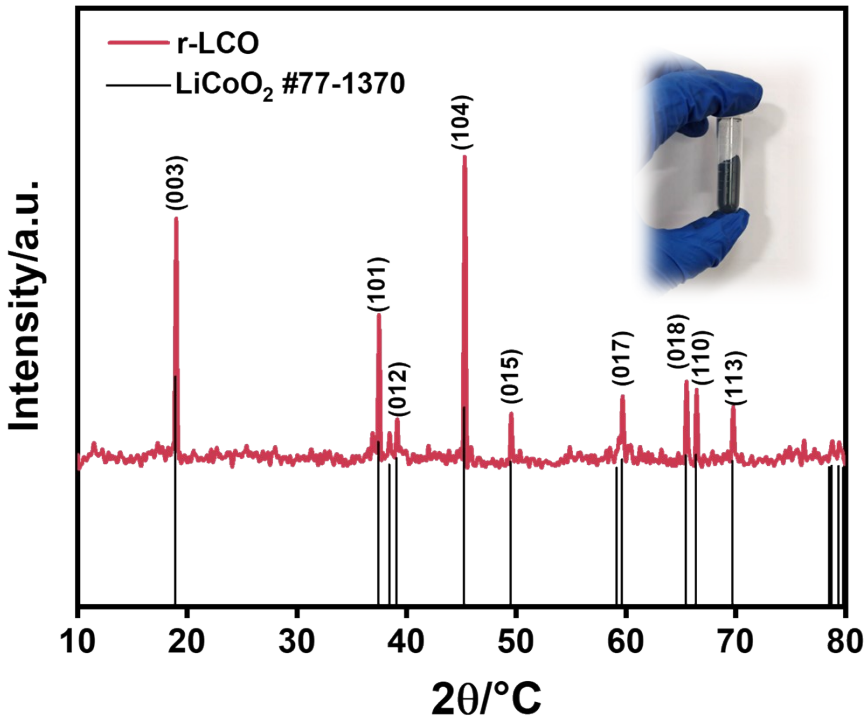

Figure S13. XRD analysis of the obtaining lithium cobaltate.

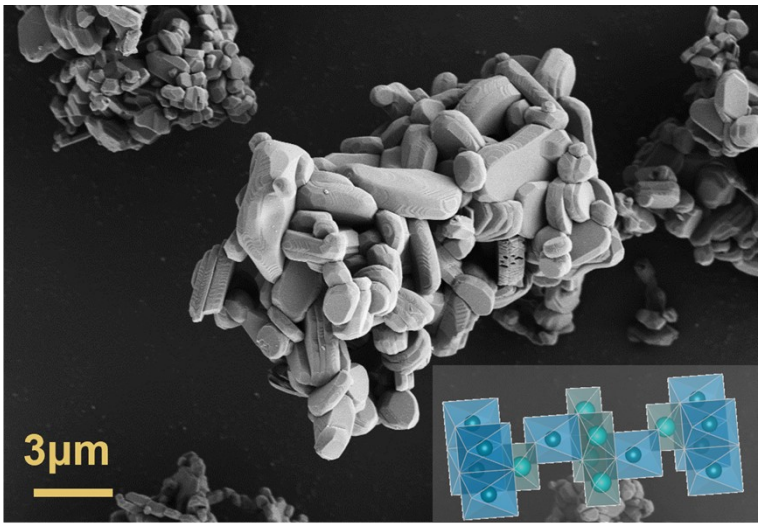

Figure S14. XRD analysis of the obtaining lithium cobaltate.

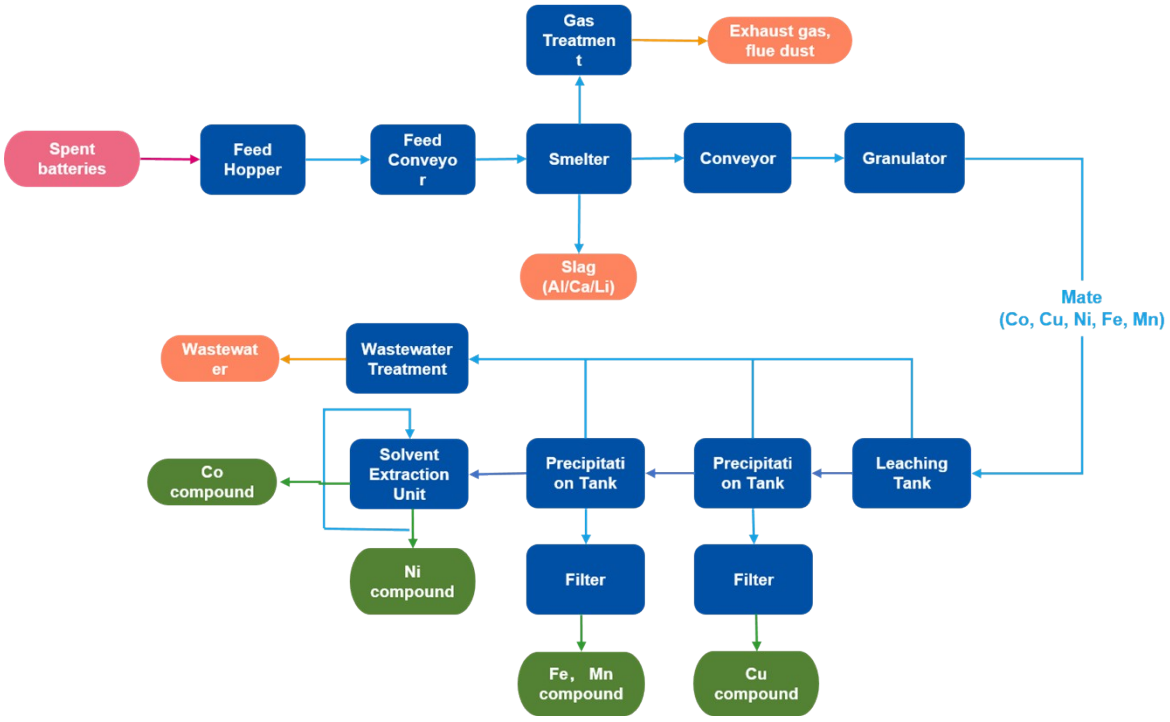

Figure S15. Process diagram of a generic pyrometallurgical recycling process.

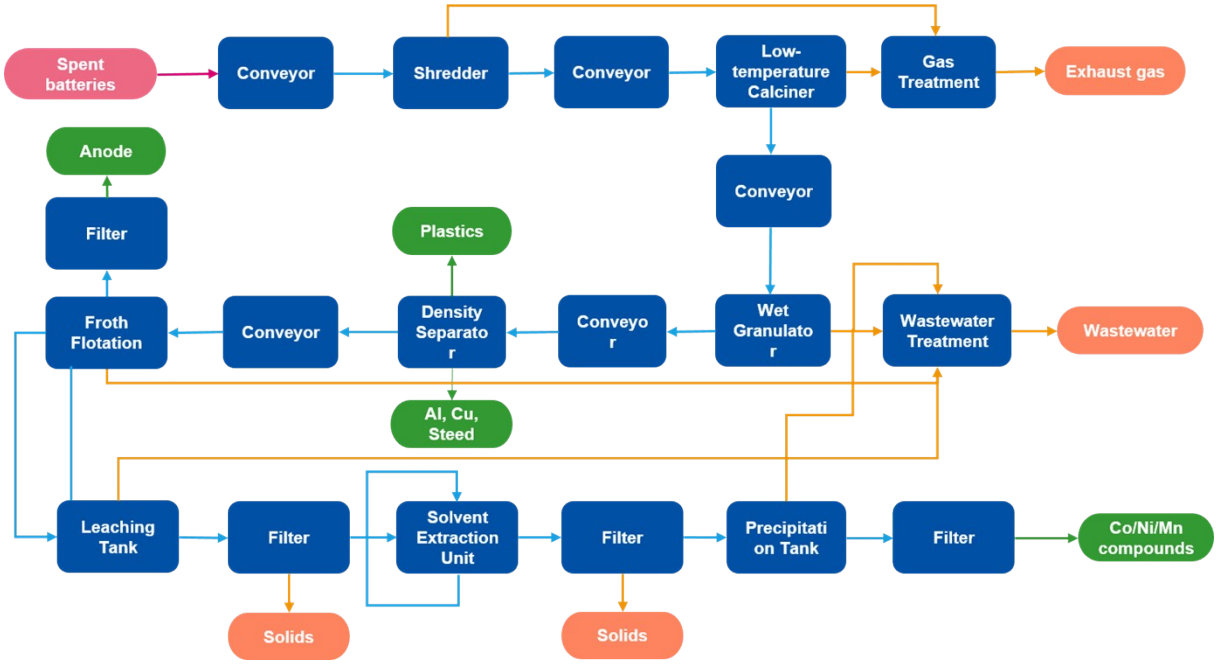

Figure S16. Process diagram of a generic hydrometallurgical recycling process.

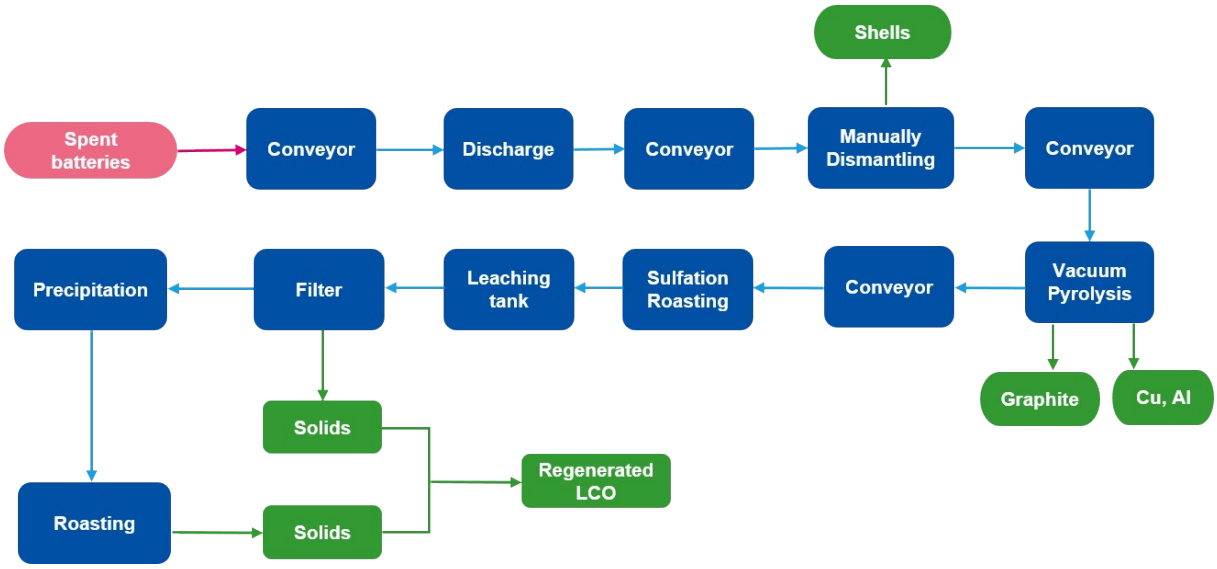

Figure S17. Process diagram of this recycling process.

Table S1. The composition of the obtained cathode powder (wt%)

Component	Co	Li	Al	Ni	Mn	Fe	S	Si	Na
Cathode material	54.39	6.74	0.08	0.06	0.01	0	0	0	0

Table S2. Materials and energy requirements to recycle 1 kg of spent batteries through different technologies (NR is not required).

	Pyrometallurgy	**Conventional Hydrometallurgy**	**This work**
Ammonium sulfate	NR	NR	0.67
Ammonium hydroxide	NR	0.031	NR
Hydrochloric acid	0.21	0.012	NR
Hydrochloric peroxide	0.06	0.366	NR
Sodium hydroxide	NR	0.561	NR
Limestone	0.30	NR	NR
Sand	0.15	NR	NR
Sulfuric acid	NR	1.08	NR
Soda Ash	NR	0.02	0.02
Lithium Hydroxide	NR	NR	NR

Lithium carbonate	NR	NR	NR
Water consumption (gal)	NR	1	1

Table S3. Value of recycled materials ($/kg).

	Cathode product	**Co^{2+} in product**	**Graphite**	**Aluminum**	**Copper**
$/kg	50	55	0.28	1.3	6.6

Table S4. Material recovered from recycling process (kg/kg spent battery).

	Pyrometallurgy	**Conventional Hydrometallurgy**	**This work**
Copper	0.169	0.169	0.169
Aluminum	NR	0.085	0.085
Graphite	NR	0.175	0.140
Co^{2+} in product	0.238	0.238	NR
Cathode product	NR	NR	0.363

Table S5. The potential revenue of three recycling processes

Materials		**Pyro**		**Hydro**		**This work**	
	Unit Prices ($/kg)	**Recycled mass(kg)**	**Revenue ($)**	**Recycled mass(kg)**	**Revenue ($)**	**Recycled mass(kg)**	**Revenue ($)**
			revenue				
Copper	**6.6**	**0.14**	**0.92**	**0.14**	**0.92**	**0.14**	**0.92**
Aluminum	**1.3**	**0**	**0**	**0.074**	**0.096**	**0.074**	**0.096**
Graphite	**0.28**	**0**	**0**	**0.175**	**0.049**	**0.175**	**0.049**
Co^{2+} in output	**55**	**0.069**	**3.80**	**0.069**	**3.80**	**0**	**0**
Cathode product	**50**	**0**	**0**	**0**	**0**	**0.30**	**15**

Text S1:

The leaching efficiencies of valuable elements:

$$\alpha i = \frac{VCi}{m\omega^i} \times 100\%$$

where Ci (g/L) signifies the element i concentration; V (L) defines the volume of the leachate; ωi (%) denotes the element i composition in the raw products; and m (g) denotes the quantity of the raw material (i).

Recovery and regenerate of $LiCoO_2$:

The water leachate was concentrated by evaporation at over 95°C, then a saturated Na_2CO_3 solution was added gradually until a Li^+ to CO_3^{2-} molar ratio reached 1:1.3, with pH adjusted to over 12. Li_2CO_3 was obtained after filtration. The Li_2CO_3 product was then dried at 90°C.

The Co_3O_4 obtained was wet-ground with Li_2CO_3 (Li/Co=1.05), and the resulting slurry was dried and further ground to ensure thorough mixing. The solid-state approach was employed to regenerate LCO by roasting the mixture at a heating rate of 10°C/min from ambient temperature to 850°C for 12 hours, resulting in the formation of r-LCO.

Text S2:

Computational details

All the calculations are performed in the framework of the density functional theory with the projector augmented plane-wave method, as implemented in the Vienna ab initio simulation package [1]. Spin polarization was also included. The generalzied gradient approximation (GGA) proposed by Perdew, Burke, and Ernzerhof is selected for the exchange-correlation potential [2]. A DFT-D3 scheme of dispersion correction was used to

describe the van der Waals (vdW) interactions in molecule adsorption [3]. The cut-off energy for plane wave is set to 500 eV. The energy criterion is set to 1E-05 eV in iterative solution of the Kohn-Sham equation. All the structures are relaxed until the residual forces on the atoms have declined to less than 0.02 eV/Å. The electron smearing width of $\sigma = 0.03$ eV was employed according to the Gaussian smearing technique. The Brillouin zone integration is performed using the uniformly distributed scattering of going through the Gamma point to select a 3x3x1 k-mesh in the Monkhorst-Pack grid to make structure optimization [4].

The charge density difference was evaluated using the formula $\Delta\rho = \rho(\text{slab}+NH_3) - \rho(\text{slab}) - \rho(NH_3)$, then analyzed by using the VESTA code [5].

[1] Kresse, G.; Joubert, D. From ultrasoft pseudopotentials to the projector augmented- wave method. Physical Review B 1999, 59, 1758-177.

[2] Perdew, J. P.; Burke, K.; Ernzerhof, M. Generalized gradient approximation made simple. Physical Review Letters 1996, 77, 3865-3868.

[3] Grimme S, Antony J, Ehrlich S and Krieg H 2010 A consistent and accurate ab initio parametrization of density functional dispersion correction (DFT-D) for the 94 elements H-Pu Journal of Chemical Physics 2010, 132, 154104.

[4] Hendrik Monkhorst, James Pack. Special points for Brillouin-zone integrations[J]. Physical Review B, 1976, 13(12): 5188-5192.

[5] Momma, K.; Izumi, F., VESTA: a three-dimensional visualization system for electronic and structural analysis. J Appl Crystallogr 2008, 41, 653-658.

Analysis methods:

The electrochemical characteristics of all cathode materials were evaluated using CR2032 button cells. A mixture of cathode material, polyvinylidene fluoride (PVDF), and acetylene black in an 8:1:1 mass ratio was combined with N-methylpyrrolidone (NMP) to create a uniform slurry. This slurry was coated onto aluminum foil, dried in a vacuum oven at 120 °C for 10 hours. The electrolyte consisted of a 1 M $LiPF_6$ solution in a solvent blend of ethylene carbonate (EC), methyl carbonate (EMC), and dimethyl carbonate (DMC) in equal volume proportions, with a polypropylene separator utilized. Electrochemical charge/discharge and rate performance evaluations were conducted in the voltage range of 3.0 to 4.5 V (*vs* Li^+/Li) using NEWARE battery test system.

The solid samples underwent examination using a Bruker D8 Advance X-ray diffractometer with Cu Kα radiation (λ=1.5406Å). The diffraction patterns were obtained by scanning the 2θ range from 10° to 80°. Additionally, XPS was employed to investigate the transformation and behavior phase formation, utilizing an ESCALAB 250Xi spectrometer from Thermo Scientific. To assess metal concentrations in the leachate, an ICP-OES analyzer (ICAP 7000, Thermofisher) was used. The morphology and elements contents in the surface of solid samples were evaluated using a 20 kV SEM, namely the Hitachi S4800 model from Japan. To investigate the thermal characteristics of the LCO and the mixture (with a mole ratio of $(NH_4)_2SO_4$ to LCO at 0.7:1 and an anode mass of 10% relative to LCO), thermal gravimetric analysis (TGA) was performed using a Pris 1 TGA instrument under an air flow environment. HSC Chemistry 9.0 program was used to determine thermodynamic parameters such as free energy changes, standard Gibbs enthalpy changes, and equilibrium composition of processes involving $LiCoO_2$, $(NH_4)_2SO_4$, and C. The morphologies and crystal structures of spent LCO

and roasting slag were analyzed by high resolution transmission electron microscopy (HRTEM, JEOL, JEM-2100 plus).

Text S3:

Economic and environmental analysis:

The EverBatt model can perform techno-economic and life-cycle analysis of three types of spent battery recycling processes: pyrometallurgy (Pyro), hydrometallurgy (Hydro), and this work in manuscript. It is a closed-loop battery recycling cost and environmental impacts model developed by Argonne National Laboratory. We select the Pyro and Hydro in the EverBatt model as a reference to assess this work (our cathode recycling (C-$(NH_4)_2SO_4$ synergistic roasting recycling processes)) in respect of energy consumption, GHG (greenhouse gas) emissions, and economic benefits.

The recycling flow charts for the commercial pyrometallurgy, commercial hydrometallurgy in EverBatt model and our work are depicted in Figure S15, Fig. S16, and Fig. S17, respectively. The new direct recycling (This work) in the figure and the following refer to the process of C-$(NH_4)_2SO_4$ synergistic roasting to recover $LiCoO_2$.

Figure S15 depicts the process of generic pyrometallurgical recycling. In the process, the spent batteries are sent to a smelter, and the electrolyte and plastics in the batteries are burned off to supply heat; graphite/carbon and aluminum in the batteries act as reducing agent for the transition metals; Co, Cu, and Fe in the batteries end up in the matte; and the rest of the materials, including oxidized aluminum end up in the slag. The Co/Cu/Fe matte is then further leached by acid followed by solvent extraction and precipitation to produce cobalt and nickel compounds that can be used for new cathode materials production. It should be noted that

lithium in the slag can potentially be recovered.

Figure S16 depicts the process of the generic hydrometallurgical recycling process. Firstly, the discharged and dissembled spent batteries are shredded and then undergo a low-temperature roasting process to burn off the binder and electrolyte, followed by several physical separation processes to separate out aluminum, copper, and steel as metal scraps and plastics. Then the anode is obtained after flotation and filtering, and a leaching process followed by solvent extraction and sometimes precipitation to produce Co compounds, and potentially lithium carbonate for new cathode material production.

Fig. S17 depicts the direct recycling process of C-$(NH_4)_2SO_4$ synergistic roasting. In this process, the spent LIBs are discharged, disassembled, and undergo a series of physical separation processes to obtain plastics, metals, anode material, and cathode material. Subsequently, the $(NH_4)_2SO_4$, the anode power and the cathode powders are mixed and roasted, and the roasted product is filtered and chemically precipitated to obtain the $LiCoO_2$ precursor, realizing the regeneration.

Evaluation of energy consumption and greenhouse gas emissions (GHGs)

Materials input

The materials requirements for the three recycling technologies are summarized in Table S3. The materials requirements for the pyrometallurgical and hydrometallurgical processes are obtained from EverBatt. The materials requirements for this work are obtained according to our experimental procedure. In the evaluation of the recycling process, the energy consumption and greenhouse gas emissions in the material production process are also considered

Energy input

In order to calculate the impact of the various energy consumed in the process on the life cycle environment, the life cycle analysis will consider the environmental impact related to upstream fuel production and power generation, as well as the environmental impact related to on-site fuel combustion.

Process emissions

In the evaluation of greenhouse gas emissions EverBatt model also consider the environmental impacts related to process emissions. These GHG emissions are not caused by fuel combustion but are produced by the combustion of materials in the battery. GHG emissions are calculated based on 100-year global warming potentials from the fifth assessment report of the Intergovernmental Panel on Climate Change.

Evaluation of potential revenue

The revenue calculation was based on the sales of recycled materials. The prices and the quality of the various materials recovered are obtained from EverBatt and listed in Table S4-S6. Revenues are calculated as:

$$Revenue = \sum mi \times upi$$

Where m_i (g/L) is the mass of material i recovered from spent batteries; and up_i is the unit price of material i as shown in Table S4.